Suess, E., von Huene, R., et al., 1990
Proceedings of the Ocean Drilling Program, Scientific Results, Vol. 112

28. VOLCANIC ASH FROM LEG 112 OFF PERU[1]

André Pouclet,[2] Hervé Cambray,[2-3] Jean-Paul Cadet,[3] Jacques Bourgois,[3] and Patrick De Wever[4]

ABSTRACT

During Leg 112 off Peru, volcanic material was recorded from middle Eocene to Holocene time. The petrographical and chemical composition of tephra is consistent with an origin from the Andean volcanic arc. The amount and thickness of ash layers provide valuable evidence for explosive volcanic episodicity. The first indication of volcanism was found in mid-Eocene sediments. Three volcanic pulses date from Miocene time. Two intense episodes took place in upper Pliocene and from Pleistocene to Holocene time. Pliocene-Pleistocene tephra are restricted to the southern upper-slope and shelf sites, indicating a removal of the volcanic arc and the extinction of the northern Peru volcanoes.

The Cenozoic tectonic phases of the Andean margin may be correlated with the Leg 112 volcanic records. The explosive supply of evolved magmatic products succeeded the Incaic and Quechua tectonic phases.

Acidic glasses are related to both andesitic and shoshonitic series. The calc-alkaline factor (CAF) of these glasses exhibited moderate magmatic variations during middle and late Miocene time. A dramatic change occurred during the Pliocene-Pleistocene, reflected in a strong CAF increase and the appearance of potassium-rich evolved shoshonitic glasses. This took place when the Nazca Ridge subduction began. This change in the magma genesis and/or differentiation conditions is probably related to thickening of the upper continental plate and to a new configuration of the Benioff Zone.

INTRODUCTION

During Leg 112, 10 sites were drilled off Peru, between 9° and 14°S latitude, to reconstruct the tectonic and oceanographic histories of the Andean margin, which is linked to subduction of the Nazca Plate (Fig. 1). Two transects were drilled across the convergent margin from the shelf to the lower slope. The northern transect (Sites 683, 684, and 685) was surveyed during the SeaPERC cruise of the *Jean Charcot* (Pautot et al., 1986; Bourgois et al., 1986, 1988a, 1988b). The southern transect (Sites 679, 680, 681, 682, and 688) was surveyed by the *Moana Wave* (Hussong et al., 1988). Two additional sites (686 and 687) in a southernmost area were drilled into the Lima Basin on the upper slope. Quaternary to early Eocene sediments, including airfall ash layers, were penetrated in different cores.

The aim of this study is to analyze the geographical and chronological distributions and the petrographical and chemical compositions of tephra. These data provide the means, first, to obtain a record of the explosive activity of the volcanic front, and then, to examine the correlation between the pulses of volcanic activity, their magmatic geochemical features, and their association with regional tectonic events.

Extensive diagenesis is related to sediments in sulfate reduction or methanogenesis and formation of diagenetic carbonate cements (Suess, von Huene, et al., 1989). Moreover, circulation of low-chloride interstitial fluids occurred in some zones. In these conditions, post-depositional alteration may affect volcanic glass fragments and falsify the volcanic record. Hence, we note the alteration problem, and we analyze different glass-poor beds as well as glass-rich ash layers.

ASH AT LEG 112 SITES

Northern Transect

Three sites were investigated as part of the northern transect; from the upper slope to the trench: Sites 684, 683, and 685 (Fig. 2).

Site 684 is located on the slope of the Trujillo Basin, at 135 km seaward from the coast of Peru. Three holes were drilled. The deepest one, Hole 684A, was cored down to 136 mbsf, where stratigraphic sections of late Quaternary, Pliocene, and middle Miocene age were recovered.

Dispersed ashy material is present in many cores (5%–15% glass). One ash pod was found in Pliocene strata. A thin ash layer was recovered in middle to late Miocene sediments; it consists of 70% glass shards and bubble-wall fragments, with some quartz, feldspar, oxide grains, and biotite flakes in a biogenic mud.

Site 683 is located on the seaward side of the Yaquina Basin. Two holes were drilled: Hole 683A was cored down to 419 mbsf, and sediments were recovered from 403 to 488 mbsf in Hole 683B. The sedimentary sequence consists of three lithological units dating from (1) Quaternary to Pliocene, (2) middle Miocene, and (3) middle Eocene.

The sampled sequence recorded almost continuous explosive activity, with 5% to 25% of volcanic material in many cores. A millimetric ash bed was crossed in Pleistocene strata; it consists of tiny, colorless glass shards, and minor quartz and feldspar. Middle Miocene mudstone contains six ash layers (0.5–2 cm thick), consisting of 60% to 90% glass fragments with quartz, feldspar, and scarce biotite and five ash pods (25%–60% glass). One ash bed (40% corroded glass grains with illite alteration) was recovered in Eocene mudstone. This sediment, deposited before the Andean orogeny, overlies a continental basement consid-

---

[1] Suess, E., von Huene, R., et al., 1990. *Proc. ODP, Sci. Results*, 112: College Station, TX (Ocean Drilling Program).

[2] Laboratoire de Géotectonique et Pétrologie, Université d'Orléans, 45067 Orléans, France.

[3] Laboratoire de Géotectonique, Université Pierre et Marie Curie, 75231 Paris, France.

[4] Laboratoire de Stratigraphie, Université Pierre et Marie Curie, 75231 Paris, France.

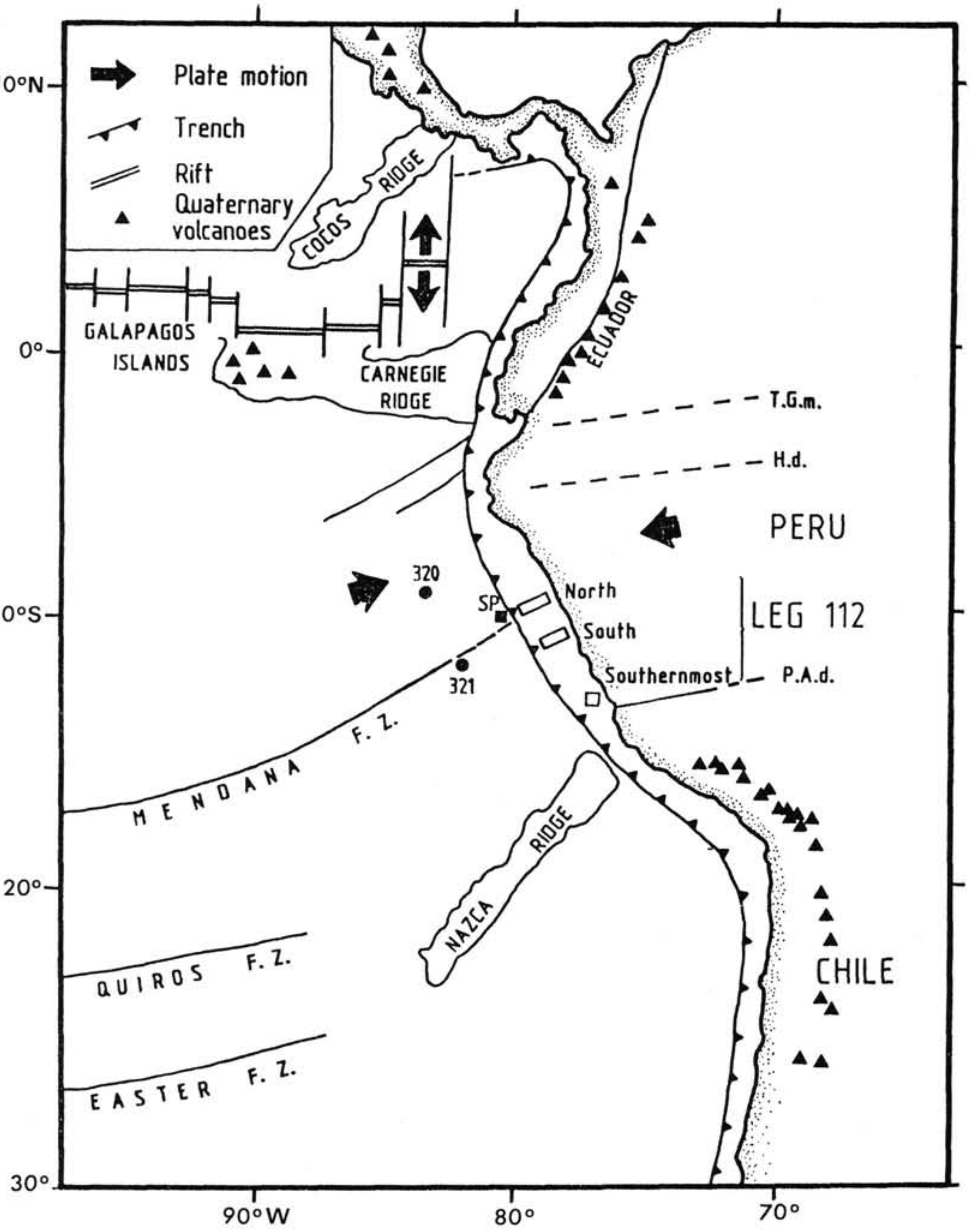

Figure 1. Geographic and structural setting of Leg 112. SP = SeaPERC cruise Mendaña box; Sites 320 and 321 of Leg 34; T.G.m. = Tumbes Guayana megashear; H.d. = Huancabamba deflection; P.A.d. = Pisco Abancay deflection.

ered a seaward prolongation of the South American continent.

Site 685 is positioned on the lower slope, at about 1200 m above the trench floor. The sediments recovered have been subdivided into two lithologic units. Unit I consists of 200 m of slope deposits dating from early Pleistocene. Sparse volcanic material (3%–6% glass) is present in some sections. Unit II, drilled to 468.6 mbsf, is considered to be an old, accreted complex of late Miocene age. Two ash layers, 0.5 cm thick and from 75% to 80% colorless glass, were recovered at 390 mbsf. The lower part contains significant amounts (20%-40%) of tuffaceous materials (colorless to pale brown glass, quartz, and feldspar fragments).

Southern Transect

Five sites (681, 680, 679, 682, and 688) were drilled along the southern transect, from the shelf edge to the lower slope.

Site 681 is the most landward at the shallowest water depth, 150 m, in the Salaverry Basin. Three holes penetrated down to 187, 143.5, and 86.4 mbsf. They recovered a Pliocene-Pleistocene sequence.

Volcanic glass is present (5%–10%) in some Pleistocene strata. Because of the high rate of sedimentation, the volcanic material is diluted by the terrigenous and biogenic sediments. Scarce, thin beds of ash-bearing mud may be encountered. However, a graded, centimeter-thick ash layer, with a sharp

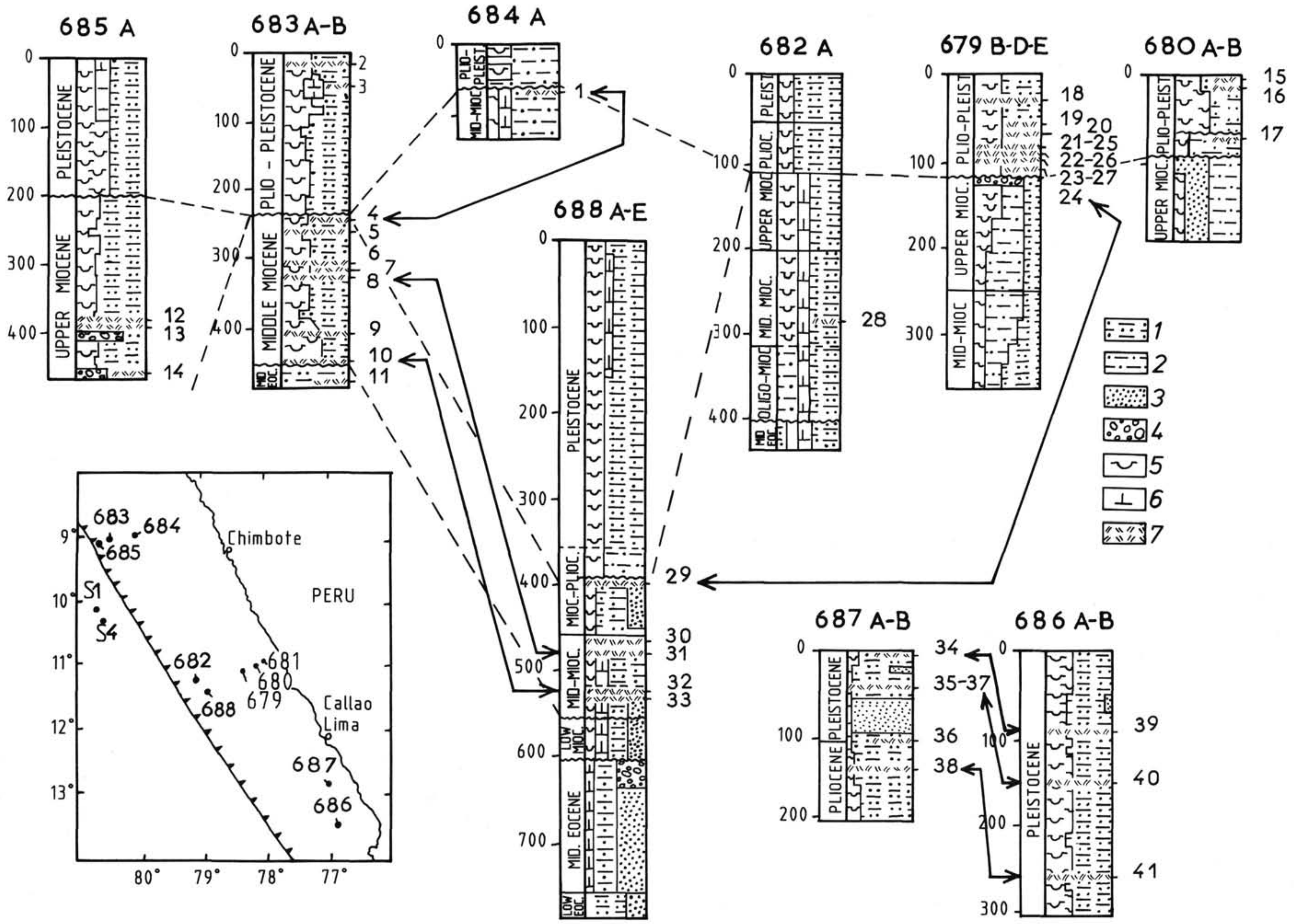

Figure 2. Simplified stratigraphic columns and location of the sites. S1 and S4 = Holes KFO1 and KFO4 of the SeaPERC cruise. Numbers are the sampled tephra. Dashed lines = stratigraphic correlations; solid lines = proposed ash beds correlations. 1, mud; 2, silt; 3, sand; 4, conglomerate; 5, siliceous ooze; 6, calcareous ooze; 7, volcanic ash.

base, was found that dates from 0.5 Ma (based on the sedimentation rate).

Site 680 was positioned on the brink of the shelf edge in the Salaverry Basin, at a water depth of 261 m. Three holes were drilled: Hole 680A at 93.8 mbsf, Hole 680B at 195.5 mbsf, and Hole 680C at 34.3 mbsf. The recovered sediments are divided into three lithologic units dating from (1) late Quaternary, (2) Pliocene-Pleistocene, and (3) upper Miocene.

The Holocene to late Pleistocene upper part of lithologic Unit I includes eight centimeter-thick (1–5 cm) ash-bearing sandy to silty mud beds with colorless glass shards and numerous feldspar fragments. Unit II is thin and devoid of significant volcanic material. In Unit III, the dispersion of rare glass fragments is explained by dilution, by detrital deposition, and by the overall poor recovery. One ash-bearing bed appears in the upper part, which had the best-recovery rates.

Site 679 is located on the eastern side of the Lima Basin at a water depth of 450 m. Five holes were drilled, with the deepest penetration at 359 mbsf. Five lithologic units have been identified, dating from Quaternary to middle Miocene.

The Quaternary to Pliocene hemipelagites are tephra-rich. A 5- to 10-cm-thick ash layer occurs near the top of all the holes. Four 2- to 10-cm-thick beds of ash-bearing or pyroclastic mud were recovered in upper Quaternary strata. Many ash pods and three beds of pyroclastic mud were recovered in Pliocene-Pleistocene strata. Three important ash layers (10-25 cm) were encountered from upper Pliocene time; these layers correlate between Holes 679B and 679D and contain 70% to 95% colorless glass shards, bubble-wall fragments, and micropumices with minor quartz and feldspar. The upper Miocene strata are more clastic, and the volcanic material is dispersed. Three pyroclastic mud beds occur in the upper part. The middle Miocene sequence is more tephra-rich and contains three ash-bearing mud beds in the upper part and five ash-bearing mud beds and some ash pods in the middle part.

Site 682 is located on the lower slope of the trench, at a water depth of 3788 m. Hole 682A was cored down to 437 mbsf, where three stratigraphic sequences were recovered.

The first sequence, dating from Quaternary to mid-Miocene, includes some reworked tephra: two ash pods were observed in lower Pliocene and upper Miocene sediments; one pyroclastic mud bed, in the deepest upper Miocene strata, contains 40% brown to colorless glass fragments and grains with minor quartz, feldspar, and oxides. Volcanic material is also scarce in the second sequence, mid-Miocene to Oligocene: one ash pod and one pumiceous pyroclastic cluster occurred in the middle Miocene strata. The third sequence, of mid-Eocene age, is nearly devoid of ash.

Site 688 is located on the lower slope, 30 km landward of the trench axis, at a water depth of 3830 m. Five holes were drilled. Holes 688A and 688C were cored with the deepest penetration at 770 mbsf. Three major lithologic units were recovered from the Quaternary to early Eocene.

As in Site 682, the Quaternary slope sediments are tephra-poor. The Miocene-Pliocene strata contains one ash layer (80% reworked and poorly sorted, large, colorless glass fragments and micropumices) and one pyroclastic mud bed. The middle to early Miocene strata contains four thin ash layers with 75% to 90% colorless glass shards, bubble-wall fragments, and minor quartz, feldspar, and magnetite. In addition, two tephra-bearing mud beds, three ash pods, and dispersed volcanic material were observed. The Eocene strata includes only some scattered shards of volcanics.

Southernmost Area

Site 687 is at the southeastern end of the Lima Basin, 50 km from shore. Two holes were drilled at a water depth of 307 m. Hole 687A was cored to a total depth of 207 mbsf, and Hole 687B was cored to 195.3 mbsf. Three lithologic units were recorded, dating from Quaternary to Pliocene.

One pyroclastic-bearing mud bed was encountered in Quaternary Unit I, near the top (altered vitric fragments and abundant feldspar grains); in addition, two white, thick (12 cm) ash layers that are correlated within the two holes (95% large and colorless glass shards, bubble-wall fragments, and pumices with minor quartz and feldspar) and one ash pod were observed in the lower part. We estimate age assignment of the ash layers as between 0.7 and 0.9 Ma. Unit II includes a reworked pyroclastic silt in the lower Pleistocene strata (45% rounded, eroded, colorless glass fragments). Volcanic material is present in Pliocene Unit III, with one 2-cm-thick ash layer (90% colorless glass shards and bubble-wall fragments with minor quartz, feldspar, and mica) and one ash-bearing mud bed.

Site 686 was positioned in the West Pisco Basin, 66 km from shore. Two holes were drilled, at a water depth of 447 m, with penetrations of 205.7 mbsf (Hole 686A) and 303 mbsf (Hole 686B). Quaternary to upper Pliocene sediments were recovered.

Both holes are well correlated. In the upper part, three beds of ash-bearing muds (20% small vitric glass shards and abundant feldspar fragments) and some ash pods were found. The middle part includes two 1- to 2-cm-thick ash layers (90% colorless glass shards and bubble-wall fragments) and two beds of ash-bearing mud. The estimated age of ash layers is 0.8 Ma (Suess, this volume). The lower part exhibits one 1-cm-thick ash layer (85% colorless glass shards and bubble-wall fragments).

SAMPLING OF ASH LAYERS AND CORRELATION AMONG SITES

Figure 2 depicts the site location and presents simplified stratigraphic columns with samples (1 to 41) collected in the different holes. Sampling corresponds to the main ash layers and to some ash-bearing beds to complete the chronostratigraphic representation. Site 681 was not selected because the same ash deposition occurred in better conditions at Site 680. Table 1 gives locations of samples and their descriptions.

On the basis of the textural and compositional characteristics, 80% of the ash samples belongs to the Type I ash-deposition of Huang (1980): discrete ash layers from single eruption with weak mixing, good sorting, and single chemical composition (see below). The others are more or less reworked or belong to Type II: mixed ashes from frequent, close-spaced eruptions and/or synchronous eruptions from multiple chambers.

The ash-layer lithology, morphometry, and mineralogy are used together with chemical composition (see below) to correlate some tephra beds. This is the case between the northern and southern transects in mid-Miocene strata (Sites 683 and 688). Ash correlation among Sites 688 through 679 allows us to determine accurately the Miocene-Pliocene hiatus. We noticed that the Pliocene-Pleistocene tephra vanishes seaward, with the disappearance of ash layers from the shelf (Site 679) to the lower slope (Site 688). This indicates poor westward transport of ash airfall or an increasing distance for the volcanoes. In contrast, the most important Miocene ash record in the westernmost sites can be explained by either more volumetrically important explosive activity, a changing of wind direction, or, more likely, proximity to the volcanic arc.

The southernmost Sites 687 and 686 contain exactly the same volcanic deposits. The 0.8-Ma ash layer characteristics seem to indicate a supplying of the volcanic material northward (marine currents ?). This is improbable, as the nearest volcanoes are located in the south east. A differential settling may be invoked.

EXPLOSIVE VOLCANISM RECORD

Many scientists assume that the record of explosive volcanic activity on land can be read, with certain limitations, in the distribution of ash in deep-sea sediments (Donnelly, 1974; Kennett and Thunell, 1975; Ninkovich and Donn, 1976; Hein et al., 1978; Cadet and Fujioka, 1980; Cadet et al., 1981 and 1982; Pouclet et al., 1985a and 1985b).

To investigate the history of explosive volcanism off Peru, we wanted to take into account all the ash layers as well as ash pods and mixing layers, if the smear-slide content of glass was more than 60%. We divided the sedimentary column into intervals of 0.5 Ma, using sedimentation accumulation curves that had been established from biostratigraphic data. For each interval, we plotted the number of ash layers and the total thickness of ash vs. time, after adjusting for the degree of core recovery.

Although this relatively simple method of recording explosive volcanism can provide more complete results than those obtained on land, where erosion destroys important exposures, it is limited by four main factors:

1. In deep-sea sediments, we find mainly silicic glass carried by strong explosive volcanism.
2. The direction of winds, and to a lesser degree, marine currents could alter the validity of results. The low atmospheric prevailing winds along the coast of Peru are westerly ones; for strong explosions, like the Atitlan-caldera eruption in Central America, ashes were uniformly distributed in the East Pacific and in the Gulf of Mexico, without important wind effects (Ledbetter, 1985).
3. Sedimentary environment is important and includes turbidity currents, sedimentary erosion, bioturbation, and deposition energy. All Leg 112 sites are disturbed by sedimentary hiatuses, and Sites 682 and 688 show evidence of slumps. Certainly, this is the most important limitation for this study, because recent K/Ar dating of ashes (Suess, this volume) indicates few redeposited ash layers, which are very difficult to find by any other method.
4. Diagenesis and alteration of glass might be a significant process in the disappearance of ash layers (Hein and Scholl, 1978), which depend not only on age, but also on heat flow and nature, size, features, interstitial fluids, and the sedimentary environment of glass. Petrographical observations and chemical analyses of Leg 112 tephra show that glass fragments underwent common alteration with hydration and smectite coating. The Eocene glasses have even been altered to illite. But, in spite of these modifications, volcanic material is always recognizable.

Pattern of Explosive Volcanic Activity

Figure 3 depicts the time-reliable record of the explosive volcanic activity, in number and thickness of ash layers.

In the northern transect, sparse ash layers in middle Eocene time were followed by three Miocene explosive activities: from 17-16, 13-12, and 10-8 Ma. The most recent sediments contain little volcanic material—a few late Quaternary ash deposits were observed.

Three Miocene volcanic phases also were found in the southern transect. After a period of quiescence during the late Miocene, an intense volcanic episode extended throughout the late Pliocene (3.5–2 Ma). Volcanic activity ceased during early Quaternary and began vigorously again in the Holocene.

The southernmost sites, which reached only to the top of the Pliocene, show an important Quaternary volcanic activity.

The intense Pliocene-Quaternary activity in the southern sites (up to 60 cm of tephra per 0.5 Ma in upper Pliocene), was not recorded in the northern ones. This difference is apparently related to the volcanic gap of the northern Peruvian Andes, known today between 3° and 16°S.

GEOCHEMISTRY AND MINERALOGY OF ASHES

Forty-one samples were selected for chemical analyses. These were taken from nine sites and 16 holes to give a representative chronological record of the magmatic characteristics from middle Eocene to Holocene. We used a Camebax electron-probe microanalyzer (EPMA) (CNRS-University-BRGM, Orléans, France) at an accelerating voltage of 15 kV, a sample current of 4 nA, a beam diameter of 1 to 10 μm, and a time count of 6 to 10 s. Measurements were corrected by using high-quality synthetic glasses to obtain an internally consistent analytical population.

A total of 295 analyses were performed on glass shards, bubble-wall fragments, and micropumices. Moreover, 54 magmatic minerals were analyzed. Some are included in glass fragments that were analyzed together. In addition, we obtained samples of the three ash layers from two cores of the SeaPERC cruise, off Peru (Pautot et al., 1986; Coulais, 1987) (S1 and S4 in Fig. 2). Twenty-eight analyses were obtained using the same procedure. Table 2 presents a selection of analyses, including the different compositions and ages.

Significances of Analytical Results

Microprobe analyses were performed with as low a sample current and a count time as possible: a 1-μm focused beam (which was necessary to analyze tiny fragments) or a 5- to 10-μm defocused beam. There is a clear spread in the results: the focused beam analyses indicate silica and alumina enrichment, and a lessened alkali content. To standardize the results, we obtained high-quality synthetic glasses of known composition. The 5- to 10-μm beam analyses were satisfactory. A more defocused beam (10–20 μm) was not necessary. Some results were also collected with the electron dispersive system (EDS) and by using an electron microscope. Raw data were corrected to allow for comparisons with shore-based data and different deep-sea glass analyses.

Even with corrections, the total amount of components of oxides averages 93% to 97%. The deficit comes from the initial volatile component and from hydration in seawater. The initial volatile component (magmatic volatile content and contamination during volcanic processes) may be as high as 5%, which we measured for recent land pumices and glass shards of dacitic to rhyolitic composition, collected in Guatemala and Costa Rica (our unpubl. data). Previous studies (Scheidegger et al., 1978; Ninkovich, 1979; Cadet et al., 1982; Pouclet et al., 1985a, 1985b) showed that hydration occurs rapidly (less than 400,000 yr) to reach a saturation point of 4% to 5% in a transparent glass. Beyond this point, phyllitic secondary products developed into the glass. Only apparently fresh Leg 112 glasses were analyzed. We calculated the correlation coefficients between the analytical deficit and oxides as follows: SiO_2, 0.319; TiO_2, 0.213; Al_2O_3, −0.002; FeOt., 0.164; MnO, −0.067; MgO, 0.110; CaO, 0.090; Na_2O, −0.004; and

Table 1. Core location and petrographic and chemical features of the sampled tephras.

Sample number	Core, section, interval (cm)	Age group	Lithology (% sand-silt-clay)	Glass (%)	Volcanic glass Type	 Medium size range in μm (extra-range)	 SiO_2 range (raw data)	 Potassic group	Notes, free crystals
	684A								
1	7H-3, 105–107	4	10-85-5	70	sh, bw, pm, gr	50–120	72.2–75.3	C	Oligoclase, biotite, oxides
	683A								
2	4H-3, 131.5–133.5	1	45-40-15	40	sh, gr	30–80	69–72.1	C	Ash pod, distant eruption
3	7H-5, 128–130	1	0-55-45	5	sh, gr	20–40	69–74	D	Rare and dispersed ash; san., and.
4	27X-1, 23–25	4	5-40-55	50	sh, bw	40–120	74–75.7	C	Na-san.
5	29X-1, 43–44	4	10-90-0	90	sh, bw, pm	60–120 (220)	73.4–74.9	C-B	And., biotite
6	34X-4, 85–87	5	50-40-10	80	sh, bw, pm	50–100 (160)	73.5–74.8	C	2-cm-thick layer; olig., biotite
7	34X-4, 122–124	5	0-40-60	10	sh, gr	20–80 (150)	73.7–75.2	C	San.
8	37X-2, 85–87	5	50-45-5	60	sh, bw, pm	20–100	71.8–73.7	C	K-and.
9	44X-6, 17–19	5	10-90-0	80	sh, bw	20–80	72.5–74.7	B	Rounded shards; and.
	683B								
10	6X-3, 6–9	6	60-35-5	70	sh, bw, pm	80–200	73.6–75.7	C	Nearby eruption; and., ilmenite
11	9X-CC, 26–28	7	5-55-40	30	sh, gr	15–80	70–73	C	Illite alteration, rounded shards; and., san.
	685A								
12	43X-1, 3–5	4	55-30-15	75	sh, bw, pm	40–120	64.1–71.4	B-C	Cogenetic differentiated glasses
13	43X-CC, 19–20	4	85-10-5	80	sh, bw	30–110	72.8–73.7	C	0.5-cm-thick ash layer
14	50X-1, 45–47	4	20-40-40	20	sh, bw	30–80	71.3–73.3	D-C	Rare Fe-rich glass, numerous fedspars, and., olig., K-anorth., Na-san.
	680A								
15	1H-1, 125–127	1	0-25-75	10	sh, bw	30–120	69.1–72.1	D	Labrador
16	2H-1, 4–6	1	40-45-15	20	sh, bw	50–80	73.8	D	And., olig., Na-san., san.
	680B								
17	8H-3, 23–25	2	0-65-35	15	sh, gr	10–80	70.7–72.5	C-D	Ash pod; olig.
	679B								
18	4H-4, 32–34	1	10-60-30	45	sh, bw	50–150	69.5–70	D	
19	7H-5, 25–27	1	0-60-40	30	sh	10–40	67.8–69.8	D	And., olig.
20	8H-6, 14–16	1	0-10-90	40	sh, bw	20–80 (150)	69.8–73.8	D-C	Heterogeneous glasses; and., anorth., san.
21	10H-2, 18–20	2	40-40-20	95	sh, bw	70–220	70.3–71.8	D	
22	10H-3, 126, 128	2	20-40-40	95	sh, bw, pm	80–200	73.7–75.6	D-C	
23	10H-4, 99–101	2	0-50-50	40	sh, gr	10–40 (120)	64.3–74.3	D-C	Heterogeneous glasses; albite
24	12H-3, 119–121	3	10-65-25	40	sh, bw, gr	50–150 (250)	69–70	D	San.
	679D								
25	9H-6, 30–32	2	15-80-5	95	sh, bw	30–120	67.8–71.1	D	White ash layer
26	10H-1, 140–142	2	30-60-10	70	sh, bw, pm	50–100	65.4–67.3	D	20-cm-thick ash layer
27	10H-3, 78–80	2	10-80-10	75	sh, bw	80–200	69–72.5	C-D	1-cm-thick ash layer; and.
28	32X-CC, 20–23	5	5-65-30	40	sh, bw, gr	20–120	56.4–71.7	C-D	Black pyroclastic mud, heterogeneous glasses; K-and.

Table 1 (continued).

Sample number	Core, section, interval (cm)	Age group	Lithology (% sand-silt-clay)	Glass (%)	Volcanic glass				Notes, free crystals
					Type	Medium size range in μm (extra-range)	SiO_2 range (raw data)	Potassic group	
	688E								
29	5R-3, 34–36	3	20-40-40	80	sh,bw,pm	20–220	70–71.8	D	Weakly reworked ash layer, poor sorting
30	14R-4, 12–14	5	10-85-5	85	sh,bw, gr	40–120	71–72.7	C-D	
31	15R-2, 62–64	5	5-90-5	74	sh, bw	30–110	70.6–73.4	C-D	
32	19R-3, 89–91	6	10-80-10	80	sh, bw	40–120	72.4–76.5	C	
33	20R-1,142–144	6	20-70-10	90	sh, bw	40–120	70.2–74	B-C	
	687A								
34	1H-5, 94–96	1	10-60-30	20	sh, bw	20–60	68.8–71.4	C-D	K-olig., san.
35	6H-4, 14–16	1	60-30-10	95	sh,bw,pm	100–200 (450)	70–73.2	C	12-cm-thick white ash layer
36	12X-1,121–123	1	30-20-50	45	sh,bw, gr	50–130 (500)	68.4–71	C	Reworked pyroclastic silt, rounded glass fragments; and., K-anorth., biotite
	687B								
37	6H-1, 62–65	1	40-55-5	95	sh, bw	50–100	69.7–71.5	C	2-cm-thick ash layer
38	16X-CC, 28–30	2	70-30-0	90	sh,bw,pm	80–140	69.8–73.1	C	2-cm-thick ash layer
	686A								
39	12X-3, 18–20	1	10-40-50	20	sh,bw,pm	30–80 (110)	67.22–74	C-D	Co-genetic differentiated glasses; labrador, and., Na-san.
	686B								
40	17X-3, 54–56	1	5-85-10	90	sh, bw	50–120	70.1–71.2	C	2-cm-thick white ash layer
41	29X-2, 64–66	1	5-90-5	85	sh, bw	40–160	71.3–72.7	C	1-cm-thick white ash layer
	SEAPERC								
1	KF01-2, 77–79	1	30-50-20	50	sh,bw,pm	80–250 (350)	69.7–72	C	1-cm-thick pyroclastic mud; and.
2	KF01-2, 99–100	1	40-40-20	80	sh, bw	100–200	70.4–72	C	1.5-cm-thick ash layer
3	KF04-1,114–115	1	40-40-20	80	sh,bw,pm	60–250 (350)	70.3–72.1	C	1.5-cm-thick ash layer

Age groups: 1 = Quaternary; 2 = late Pliocene; 3 = early Pliocene; 4 = late Miocene; 5 = middle Miocene; 6 = early Miocene; 7 = middle Eocene. Percentage of glass: 10%–25% = ash-bearing mud; 25%–60% = pyroclastic mud; 60%–100% = ash layer. Glass type: sh = shard; bw = bubble wall fragment; pm = micropumice; gr= more or less corroded grain or fragment. Potassic groups: B = medium-K; C = high-K; D = very high-K. Free crystals: and. = andesine; anorth = anorthoclase; olig = oligoclase; san = sanidine.

Table 2

Sample:	1	2	3	4	5	6	7	8	9	10	11	12A	12B	12C
SiO_2	74.70	70.69	69.97	74.12	74.22	74.71	76.47	72.07	73.31	74.31	70.66	64.69	67.41	70.82
TiO_2	0.02	0.22	0.22	0.06	0.11	0.00	0.52	0.19	0.04	0.06	0.15	0.70	0.55	0.13
Al_2O_3	11.53	12.20	12.81	11.93	12.13	12.40	11.11	12.20	12.39	11.93	11.81	12.56	12.41	11.35
Fe O t.	0.65	0.94	1.34	0.85	1.03	0.68	1.42	0.94	1.19	1.06	1.46	4.31	3.44	1.95
MnO	0.00	0.00	0.03	0.00	0.22	0.05	0.16	0.00	0.00	0.00	0.03	0.53	0.05	0.00
MgO	0.08	0.03	0.19	0.09	0.17	0.07	0.20	0.22	0.28	0.12	0.19	1.21	0.46	0.16
CaO	0.71	0.96	0.41	0.74	1.10	0.86	0.32	1.13	1.72	0.91	0.78	3.45	2.26	1.19
Na_2O	3.35	3.84	2.71	2.83	2.72	3.02	2.64	3.08	2.62	2.85	2.46	2.98	2.82	2.69
K_2O	5.17	4.30	5.51	5.15	4.23	5.13	5.61	4.36	3.29	5.00	4.85	2.29	2.82	3.78
TOTAL	96.21	93.18	93.19	95.77	95.93	96.92	98.45	94.19	94.84	96.24	92.39	92.67	92.22	92.07
Potassic group:	C	C	D	C	C-B	C	C	C	B	C	C	B	B	B-C

Table 2 (continued).

Sample:	13	14	15	16	17	18	19	20A	20B	21	22	23A	23B	24
SiO_2	73.30	72.62	70.54	73.80	71.90	70.06	68.75	70.07	72.93	70.79	75.02	65.45	73.50	69.90
TiO_2	0.11	0.18	0.21	0.11	0.19	0.00	0.29	0.27	0.05	0.26	0.17	0.45	0.14	0.00
Al_2O_3	12.02	12.10	12.60	11.12	12.93	13.40	13.71	13.09	13.00	13.24	11.71	15.00	11.27	12.38
FeO t.	0.85	1.40	0.38	0.85	1.21	1.04	1.45	0.96	1.41	1.08	0.94	1.86	0.53	0.38
MnO	0.00	0.12	0.05	0.00	0.00	0.48	0.00	0.11	0.19	0.10	0.05	0.06	0.12	0.21
MgO	0.08	0.09	0.15	0.16	0.16	0.00	0.39	0.20	0.08	0.11	0.05	0.68	0.02	0.05
CaO	0.52	0.51	0.43	0.35	0.98	0.35	0.87	0.43	0.57	0.37	0.43	1.54	0.34	0.81
Na_2O	2.68	3.59	3.25	3.04	4.16	3.37	2.54	3.45	3.06	3.39	2.88	2.99	3.09	3.17
K_2O	4.77	5.32	5.40	6.37	5.18	5.91	5.09	5.48	4.57	6.08	5.58	4.93	5.20	5.23
TOTAL	94.33	95.93	93.01	95.80	96.71	94.61	93.09	94.06	95.86	95.42	96.83	92.96	94.21	92.13
Potassic group:	C	D-C	D	D	C-D	D	D	D	C	D	D-C	D	C	D

Table 2 (continued).

Sample:	25	26	27	28A	28B	28C	28D	29	30	31	32	33	34	35
SiO_2	69.01	66.60	70.53	56.43	59.82	66.65	71.72	70.82	72.36	71.45	76.15	73.99	70.81	71.45
TiO_2	0.34	0.28	0.14	0.92	1.07	1.20	0.97	0.02	0.66	0.00	0.01	0.17	0.09	0.10
Al_2O_3	13.49	13.50	12.25	17.02	13.86	13.55	13.12	11.98	11.48	11.38	12.14	11.98	12.33	11.79
FeO t.	0.97	1.08	0.32	6.18	7.47	3.85	2.37	0.31	0.77	0.75	0.69	0.97	0.51	0.58
MnO	0.00	0.21	nd	0.10	0.10	0.04	0.21	nd	0.16	0.17	0.03	nd	0.00	0.03
MgO	0.26	0.20	0.14	3.11	3.19	0.37	0.08	nd	0.85	0.18	nd	0.23	0.08	0.09
CaO	0.24	0.40	0.49	5.85	4.18	2.85	0.45	0.50	0.74	0.77	0.51	1.21	0.62	0.45
Na_2O	3.56	3.38	2.95	3.71	2.84	4.12	2.73	2.78	2.89	2.59	2.19	2.35	2.40	3.94
K_2O	5.52	5.80	5.01	2.86	3.14	3.45	5.15	5.87	5.14	4.97	4.61	4.19	5.12	4.68
TOTAL	93.39	91.45	91.83	96.18	95.67	96.08	96.80	92.28	95.05	92.26	96.33	95.09	91.96	93.11
Potassic group:	D	D	C-D	C	C	C	C-D	D	C-D	C-D	C	B-C	C-D	C

Table 2 (continued).

Sample	36	37	38	39A	39B	39C	40	41	SP1	SP2	SP3
SiO_2	70.18	71.47	71.29	67.22	71.03	73.41	70.90	72.10	71.16	71.07	70.86
TiO_2	0.23	0.10	0.04	0.29	0.31	0.00	0.30	0.08	0.01	0.00	0.00
Al_2O_3	12.29	13.47	12.20	14.26	13.46	12.50	13.56	12.33	12.52	12.40	12.60
FeOt.	1.07	1.04	0.49	2.01	0.60	0.62	1.00	1.09	0.79	0.57	1.01
MnO	0.00	0.03	0.04	0.17	0.10	0.02	0.00	0.00	0.07	0.01	0.16
MgO	0.24	0.19	0.10	0.47	0.13	0.14	0.25	0.20	0.00	0.00	0.00
CaO	0.49	1.07	0.54	1.76	0.60	0.78	0.99	0.75	0.92	0.95	1.02
Na_2O	3.43	3.70	3.74	3.68	2.42	2.74	3.35	3.57	3.84	3.43	4.04
K_2O	4.67	4.08	4.51	3.54	4.99	5.96	4.04	4.24	4.03	4.00	4.27
TOTAL	92.60	95.15	92.95	93.40	93.64	96.17	94.39	94.36	93.34	92.43	93.96
Potassic group:	C	C	C	C	C-D	D	C	C	C	C	C

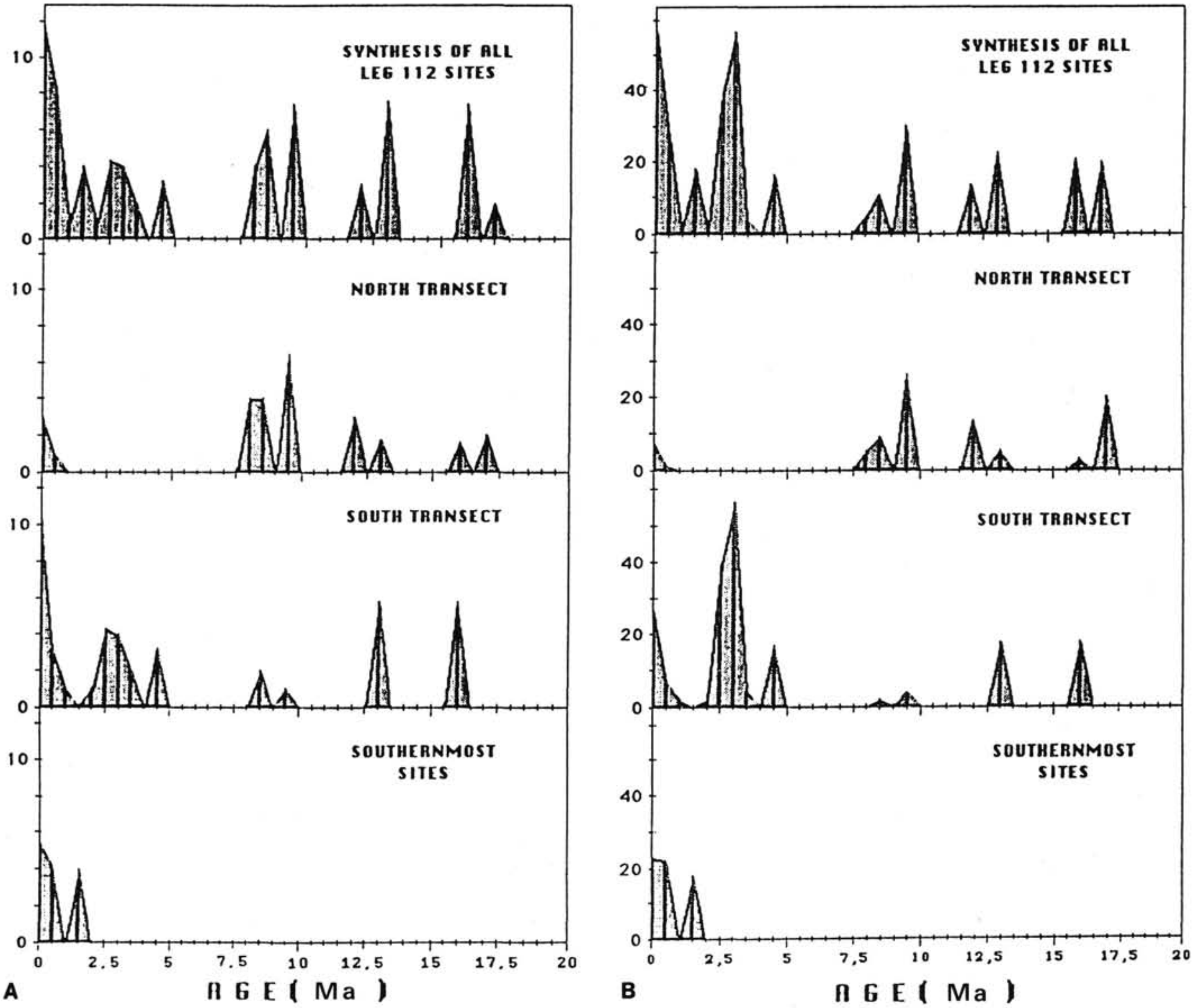

Figure 3. Time-reliable record of the explosive volcanic activity. A. Number of ash layers per 0.5-m.y. interval. B. Thickness of ash layers in centimeters per 0.5-m.y. interval.

K_2O, 0.124. One of our main findings is that no correlation can be inferred between the deficit and the alkali content. We conclude that these variations in alkali content in the glass analyses are statistically significant in terms of magma composition.

To be sure of the analytical procedure, we conducted a Link System EDS element cartography. We obtained two results. First, the glass fragments show a chemical homogeneity if we include more than a 2-μm^2 area. Second, the margin of acidic glass shards does not exhibit any chemical variation, except in a less than 5-μm rim of some bubble walls. The glass fragments were cleaned before mounting. Using the ultrathin-section technique (Eberhart and Triki, 1972; Ehret, 1985) with Miocene glass shards, we observed an outer-surface skin of illite and halloysite, precisely as in the previous study of Imbert and Desprairies (1987). The apparent freshness of the glass-fragment border may result from the nonadherence of the external alteration pellicle, as has been experimentally demonstrated with andesitic and rhyolitic glasses (Thomassin, 1984). Considering the composition of this pellicle, we think that the hydrolysis of the silicic glass leads to leaching of large ions: sodium, potassium, magnesium, and calcium.

Hence, we collected "fresh" and hydrated glasses from all Leg 112 cores, from Quaternary to early Miocene. Only the Eocene samples were gave poor results, as the glass fragments were almost entirely altered into illite.

Chemical Compositions of Glasses

All chemical compositions are related to calc-alkaline series fractionation (Fig. 4). Silica ranges from 56.4 to 76.5. Alkalies range from 4.5 to 6.4 in basic glasses, and from 5.3 to 10 in acidic glasses. The $Na_2O + K_2O/K_2O$ ratio is potassic and decreases from low-silica to high-silica compositions (average 2.1 to 1.7). All iron was calculated as FeO; the iron content was very low in acidic glasses, and this did not affect

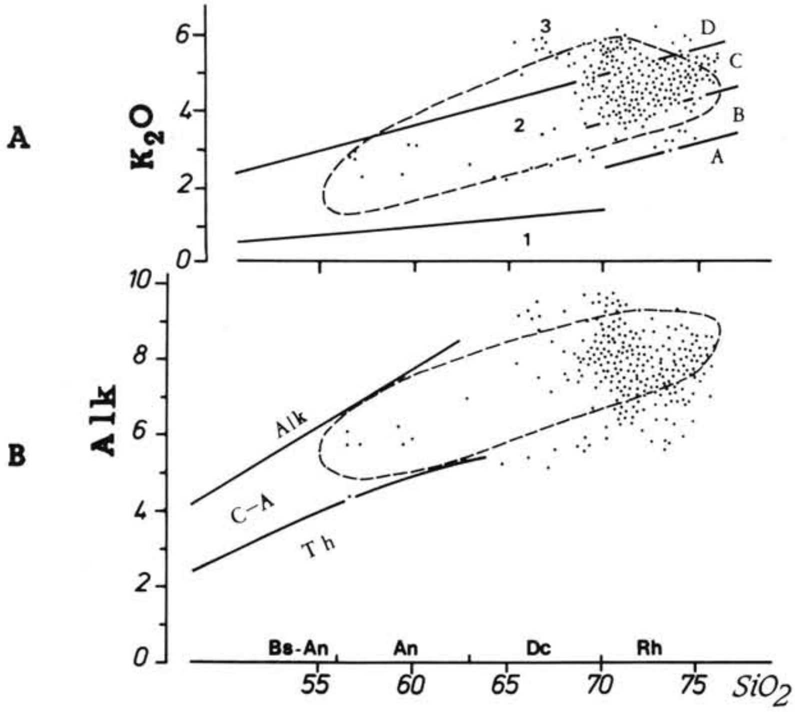

Figure 4. K_2O-SiO_2 (A) and Alkali-SiO_2 (B) diagrams of all the analyzed glasses from raw data. The depicted area corresponds to the Peruvian calc-alkaline volcanic rocks. 1, low-K andesite series; 2, andesite series; 3, shoshonite series. A, low-K group; B, medium-K group; C, high-K group; D, very high-K group. Th = tholeiitic series area; C-A = calc-alkaline series area; Alk = alkaline series area. Bs-An = basaltic andesite; An = andesite; Dc = dacite; Rh = rhyolite.

the chemical composition significantly. Eight analyses registered andesitic compositions ($56.4 < SiO_2 < 63$); these glasses, together with acidic glasses, were found in middle and upper Miocene strata of the trench sites (682 and 685). About 21% of these acidic glasses has a dacitic composition ($63 < SiO_2 < 70$) and 79% is rhyolitic ($SiO_2 > 70$).

For the SiO_2/K_2O diagram (Fig. 4B), andesitic glasses belong to the medium-potassic andesitic series. Acidic glasses partly belong to the same series, but also to the shoshonitic series. A schematic separation giving three categories, low-potassium (A), medium-potassium (B), and high-potassium (C) was determined, using volcanic ashes of Central America from Legs 66, 67, and 84 (Cadet et al., 1981, 1982; Pouclet et al., 1985a). The glasses from Leg 112 are more alkalic and more potassic. About 10% of the acidic glasses belongs to the medium-potassium group, 70%, to the high-potassium group, and 20%, to a very high-potassium or shoshonitic group (Group D).

The $Na_2O + K_2O/K_2O$ ratio decreases from Groups B and C to Group D. This ratio averages 2.1 to 1.6 in dacitic compositions and 1.7 to 1.55 in rhyolitic compositions. This decrease results from an increase in higher potassium in the shoshonitic group.

In most cases for each sample, the analyses of different glass fragments are coherent. However, some are heterogeneous: Samples 112-685A-43X-1, 3–5 cm; 112-679B-8H-6, 14–16 cm; 112-679B-10H-4, 99–101 cm; 12-682A-32X-CC, 20–23 cm; and 112-686A-12X-3, 18–20 cm. These glasses may originate from different sources, or they may be co-genetic in a single volcanic event and related to more or less evolved liquids. This is the case for Samples 112-685A-43X-1, 3–5 cm (late Miocene dacite to rhyolite, northern trench site), 112-682A-32X-CC, 20–23 cm (mid-Miocene andesite to rhyolite, southern trench site), and 112-686A-12X-3, 18–20 cm (Quaternary dacite to rhyolite, southernmost site).

Comparison of Leg 112 Tephra with Land and Other Deep-Sea Tephras

Comparison with land volcanism is limited by the few analyses of terrestrial glasses, relative to the analyses of lavas. The chemical composition of volcanics of the central Andean volcanic arc was determined in Peru by Lefèvre (1979) and in Chile by Déruelle (1979). Two differentiated potassium-andesitic and shoshonitic series coexist. As a whole, the Leg 112 volcanic glasses plot in the same compositional area (Fig. 4). They differ from Central American ashes, which have lower calc-alkaline characters (Woodruff et al., 1979), and from some Colombia-Ecuador and Chile-Argentina products, which exhibit higher potassium contents (Drexler et al., 1980; Déruelle, 1979).

In the Mandaña area of the SeaPERC cruise (SP, Fig. 1), some ash beds were recovered in Holes KF01 and KF04. According to Coulais (1987), the upper bed may correspond to the Worzel layer-L ash (230,000 yr old). This ash, transported by the Cromwell Marine Current, may have reached the Mandaña Zone and the Leg 112 northern area, but only in small quantities (Ledbetter, 1985). The thickness of the SeaPERC ash beds is too important, and the chemical composition of glass is more alkalic than the L-ash glass (Ninkovich and Shackleton, 1975). L-ash glass was not recognized in the Leg 112 northern sites, although its occurrence cannot be precluded.

Acidic volcanic material was recorded during DSDP Leg 34, Sites 320 and 321 (Fig. 1) (Yeats, Hart, et al., 1976). A late Miocene to early Pliocene, clear siliceous ash layer from Site 321 may be of Peruvian origin, according to Donnelly (1976).

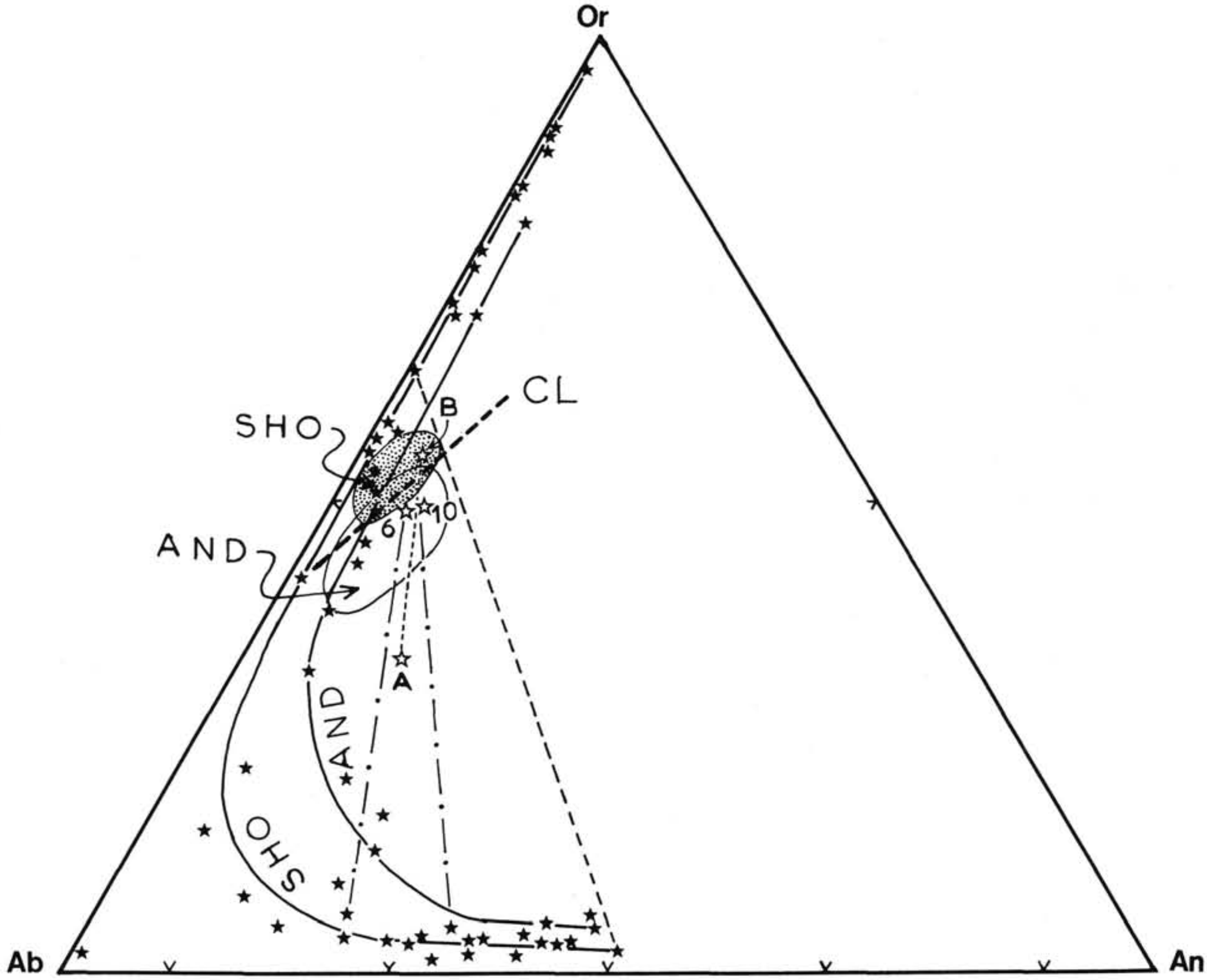

Figure 5. An-Ab-Or diagram. Closed stars = feldspar analyses; open stars = glass analyses: Samples 6, 10, and 39 with 39A (A) and 39B and C (B) analyses. AND = andesitic series: feldspathic trend (solid line) and evolved glass compositions (open area). SHO = shoshonitic series: feldspathic trend (solid line) and evolved glass composition (stippled area). CL = plagioclase-alkaline feldspar cotectic line. Light dashed line = coexisting glasses (Sample 39). Dashed and dotted line = glass, including feldspar (Samples 6 and 10). Heavy dashed line = coexisting coupled feldspars (Sample 39).

However, in the ocean-plate sites, an East Pacific Rise origin of acidic tephra may be considered in Paleocene to Miocene time (Bonatti and Arrhenius, 1970).

Chemical Compositions of Minerals

The mineral composition of samples were determined during the electron-microprobe investigation one. A total of 59 were analyzed: 52 feldspars, six biotites, and one ilmenite. Quartz and authigenic calcite and pyrite were common. We noticed the lack of muscovite, pyroxene, and amphibole. In most of the ash layers, quartz and feldspar fragments have the same size as glass fragments and originate from the same explosive event.

The composition of plagioclases ranges from andesine to potassium-oligoclase, and that of alkaline feldspars, from anorthoclase to sanidine. Some feldspars included in rhyolitic glass were analyzed: Sample 112-683A-34X-4, 85–87 cm (An, 24.3; Ab, 72.6; Or, 3.1) and Sample 112-683B-6X-3, 6–9 cm (An, 33.6; Ab, 61.9; Or, 4.5). In the An-Ab-Or diagram (Fig. 5), glass compositions of these samples plot on the plagioclase side of the plagioclase-alkaline feldspar cotectic line (James and Hamilton, 1969). This is consistent with the liquid-feldspar equilibrium. Application of the Kudo-Weill (1971) and Mathez (1973) geothermometer indicates 812° to 837°C (Sample 112-683A-34X-4, 85–87 cm) and 782° to 825°C (Sample 112-683B-6X-3, 6–9 cm), under 1 to 5 kb. A high-pressure condition, especially required in Sample 112-683B-6X-3, 6–9 cm, for temperature convenience, is the most probable in a calc-alkaline magmatism.

In many ash layers, plagioclase and alkaline-feldspar fragments can be seen together. Two feldspars were associated in the same fragment of Sample 112-686A-12X-3, 18–20 cm (An, 49.8; Ab, 48.2; Or, 4.5; and An, 0.5; Ab, 31.1; Or, 64.3). Considering the tie-line in Figure 5 and the glass composition (Analyses 39B and 39C) near the cotectic line, these two minerals may have co-precipitated from a potassium-rich liquid.

A correlation exists between the compositions of glasses and feldspars. With the glasses from Groups B and C (andesite series), plagioclases are potassic and alkali feldspars are slightly calcic. With the glasses from Group D (shoshonite series), plagioclases are less potassic, and alkali feldspars are devoid of calcium (Fig. 5). This results from the chemical control of the potassium-feldspar crystallization that occurred

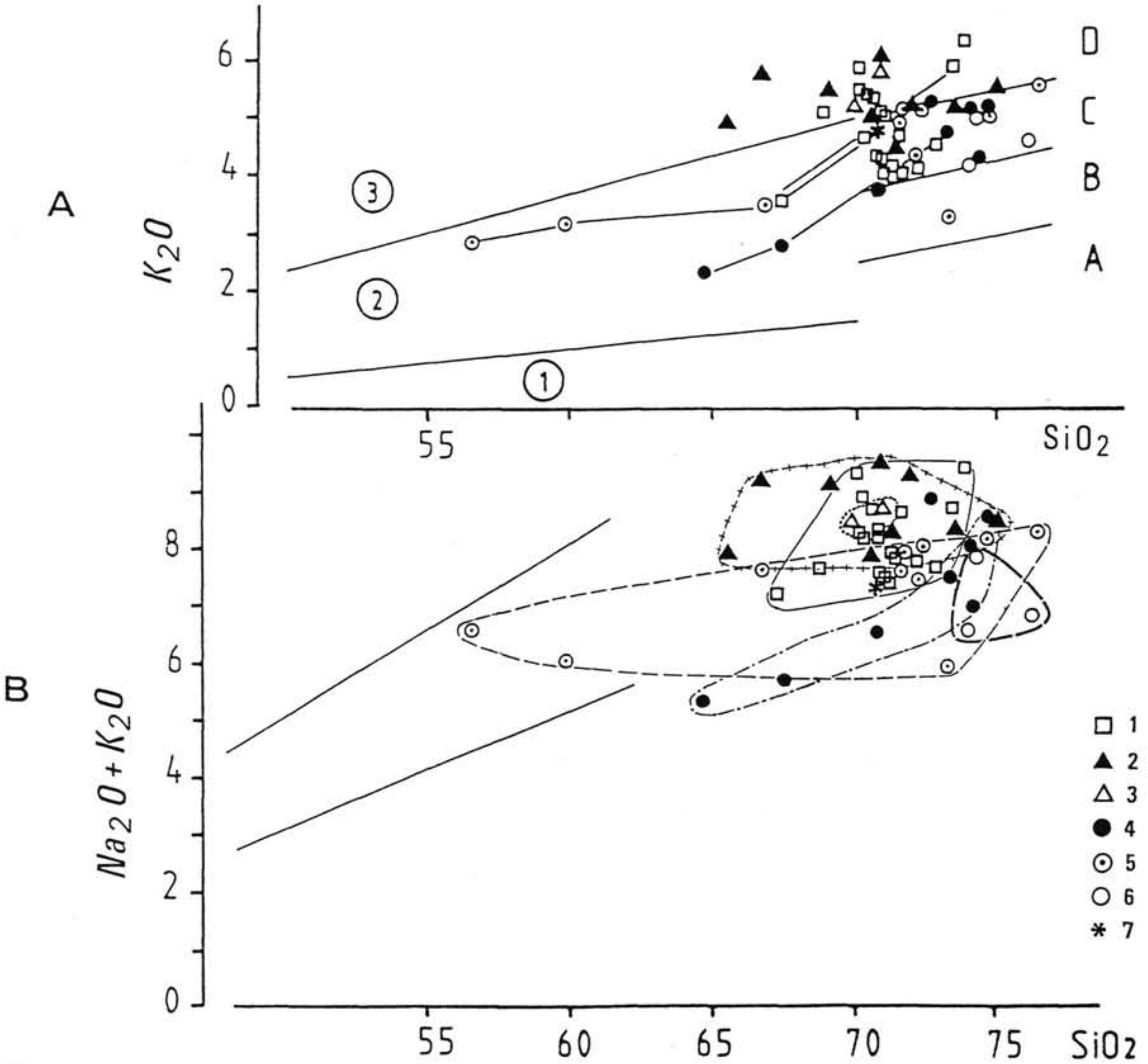

Figure 6. K_2O-SiO_2 (A) and Alkalies-SiO_2 (B) diagram. Same legend area as for Figure 4. Selected analyses for showing chronologic compositional features. Age groups: 1, Quaternary; 2, late Pliocene; 3, early Pliocene; 4, late Miocene; 5, middle Miocene; 6, early Miocene; 7, middle Eocene.

earlier in shoshonitic magma. In the An-Ab-Or diagram, shoshonitic compositions of the acidic glasses plot near the plagioclase and alkali-feldspar cotectic line and on the alkali-feldspar side.

Biotite flakes were analyzed in Samples 112-683A-29X-1, 43–44 cm, 112-683A-34X-4, 85–87 cm, and 112-687A-12X-1, 121–123 cm (Site 683, late and mid-Miocene strata; Site 687, Quaternary strata). Chemical compositions are consistent with a magmatic origin. Miocene biotites are titaniferous and magnesian (TiO_2 = 3%–4%; $Mg/Mg+Fe^{2+}$ = 61%–62%) and were crystallized under high PH_2O and fO_2 conditions (Wones and Eugster, 1965). Quaternary biotites are titaniferous and less magnesian (TiO_2 = 3.6%; $Mg/Mg+Fe^{2+}$ = 46%) and crystallized under lower fO_2.

Heavy minerals are scarce; these consist of more or less strongly altered oxides. One ilmenite was analyzed in Sample 112-683B-6X-3, 6–9 cm (early Miocene). The high hematite-molecule content, which is known in ilmenite from dacites and rhyolites, coincides with the high PH_2O conditions of the plagioclase-liquid equilibrium in this sample.

In conclusion, the chemical compositions of the magmatic minerals agree with differentiated calc-alkaline magma trends of potassium-andesitic and of shoshonitic series.

Chronological Magmatic Evolution

The age-group distinction of selected analyses is expressed in the SiO_2/alkalies and K_2O diagram (Fig. 6). The Eocene rhyolite is alkalic (Group C). The early Miocene rhyolites are potassium-rich (Group C), but relatively poor in sodium. The mid-Miocene products are generally alkali-rich (Group C). The late Miocene products are diversified and may include low alkalic compositions (Group B). All the Pliocene and Quaternary dacites and rhyolites are alkali-rich and have diversified into two potassium-andesitic or shoshonitic magmatic groups, related to the two Peruvian and north Chilian series (Lefèvre, 1979). Almost all the shoshonitic ash compositions were encountered at the shelf sites of the southern transect.

To ascertain the magmatic evolution, we performed a multidimensional statistical study. We used the method of principal component factor analysis of *n* samples and *p* variables, in this case

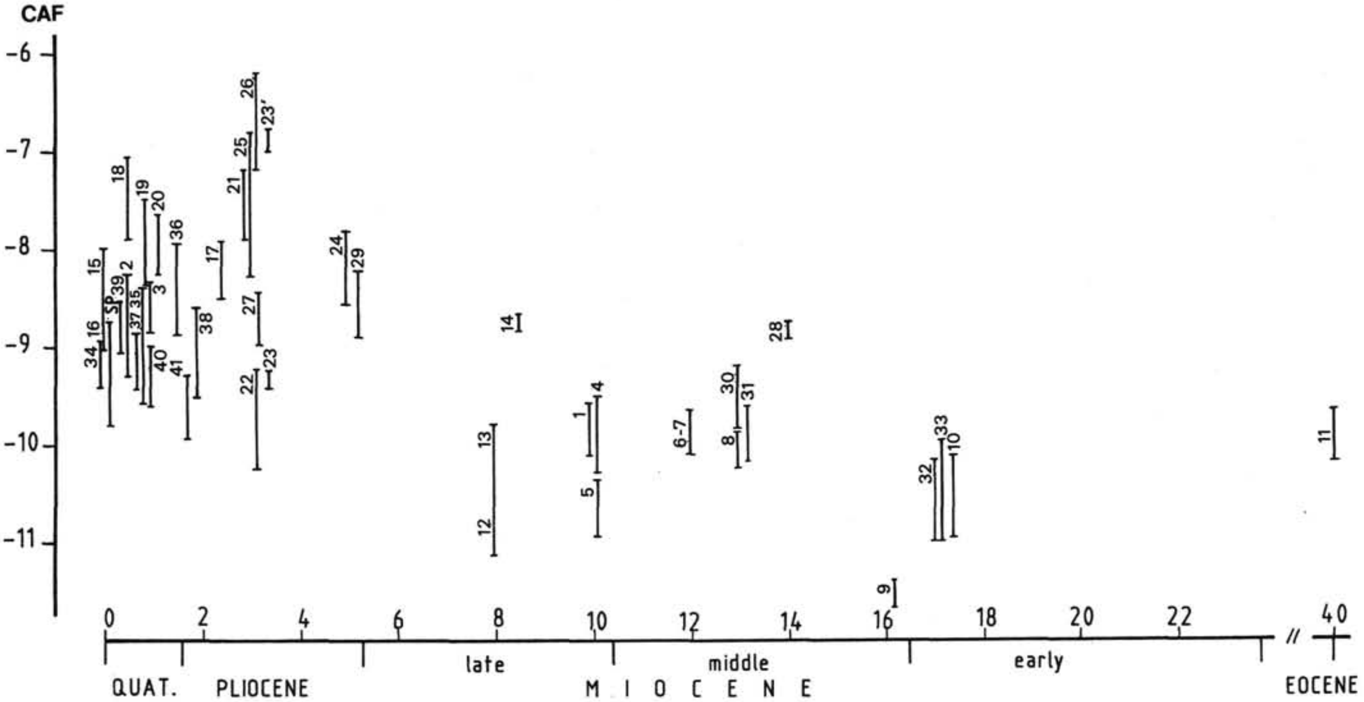

Figure 7. Chronological calc-alkaline factor (CAF) evolution for sampled ash analyses.

chemical analyses (Lebart et al., 1979). New variables, or factors correlated with the axis of the dispersion ellipse, were extracted from the correlation matrix and computed as linear transformations. These factors were arranged according to their decreasing respective contribution to the dispersion (whole variance of the population). The first factor opposes silica and alkalies to other elements and expresses the magmatic differentiation in separating andesites, dacites, and rhyolites. The second factor opposes alkalies and alumina to other elements and expresses the magmatic distinction by showing different calc-alkaline affinities in evolved glass compositions. The other factors are not significant. Theoretically, the second factor is independent of the first factor (magmatic differentiation). In practice, the best magmatic distinction concerns acidic compositions ($68\% < SiO_2 < 76\%$). In this compositional range, we can use a simplified formulation of the second factor as a calc-alkaline factor (CAF):

$$CAF = 0.8\ K_{20} + 0.7\ Na_{20} + 0.35$$

$$Al_2O_3 - 0.35\ CaO - 0.25\ SiO_2.$$

The contribution of the other elements is negligible, considering their low content in acidic compositions. The factor was calculated with water-free analyses.

In the Leg 112 dacitic and rhyolitic glasses (Fig. 7), the CAF increases from −11.5 to −6 and is less than −10 in the potassic Group B. Group C ranges from −10.5 to −8, and Group D, from −9 to −6, with the sodium-poor glasses of Group D ranging between −9 and −8.

The CAF is medium in Eocene time, low in early Miocene, high in mid-Miocene, medium-to-high in late Miocene, and medium-to-very-high in Pliocene and Quaternary time. We noticed an increase from early to mid-Miocene, a slight decrease in late Miocene, and a strong increase in early Pliocene, after a 2-Ma volcanic lull. This last evolution indicates a drastic change in the magmatic features and the eruption of very highly alkalic glasses. The CAF variations may be related to the modifications of conditions of differentiation (contamination and volatile transfer) and to the modifications of the magma genesis. These modifications result from crustal thickening or thinning, and a change in the configuration of the Benioff Zone (with different amounts of subducting sediments). The variable position of the volcanic front above the magmatic source, with respect to the continental margin and the continent-ocean limit, influences (1) the magma genesis environment (mantle source region), (2) the thermodynamic and tectonic controls of differentiation (lithospheric thickness and stress pattern), and (3) the possibility of chemical reactions (continental crust thickness).

The CAF can be used to analyze comparable acidic glass. For example, in Central American deep-sea tephra (DSDP Legs 66, 67, and 84; Cadet et al., 1981, 1982; Pouclet et al., 1985a), the CAF displays a lower calc-alkaline character. This character ranges from −14 to −12.8 in early Miocene time and from −13.3 to −9.2 in mid-Miocene to Holocene time.

DISCUSSION AND CONCLUSIONS

The time and geographic dispersion of volcanic material, together with the petrographical features and chemical compositions, clearly demonstrate that the origin of the studied tephra is the Andean volcanic arc. Volcanic fragments mostly originated from sub- to ultra-plinian acidic explosive activities. We can exclude Central America, mid-ocean ridges, or Galapagos volcanoes as a source.

A contrast exists between the Miocene and the Pliocene-Pleistocene dispersions. The lower-slope sites of Leg 112 contain many ash-bearing beds in Miocene sediments and few in Quaternary sediments; at that time, the ash deposition was restricted to upper-slope and shelf sites. From Eocene to late Miocene, the volcanic arc was active in central Peru. All the sites were supplied with volcanic material transported by aerial and marine currents from central Peru, as well as from Ecuador, southern Peru, and northern Chile. During Pliocene-Pleistocene time, volcanic activity ceased in central Peru.

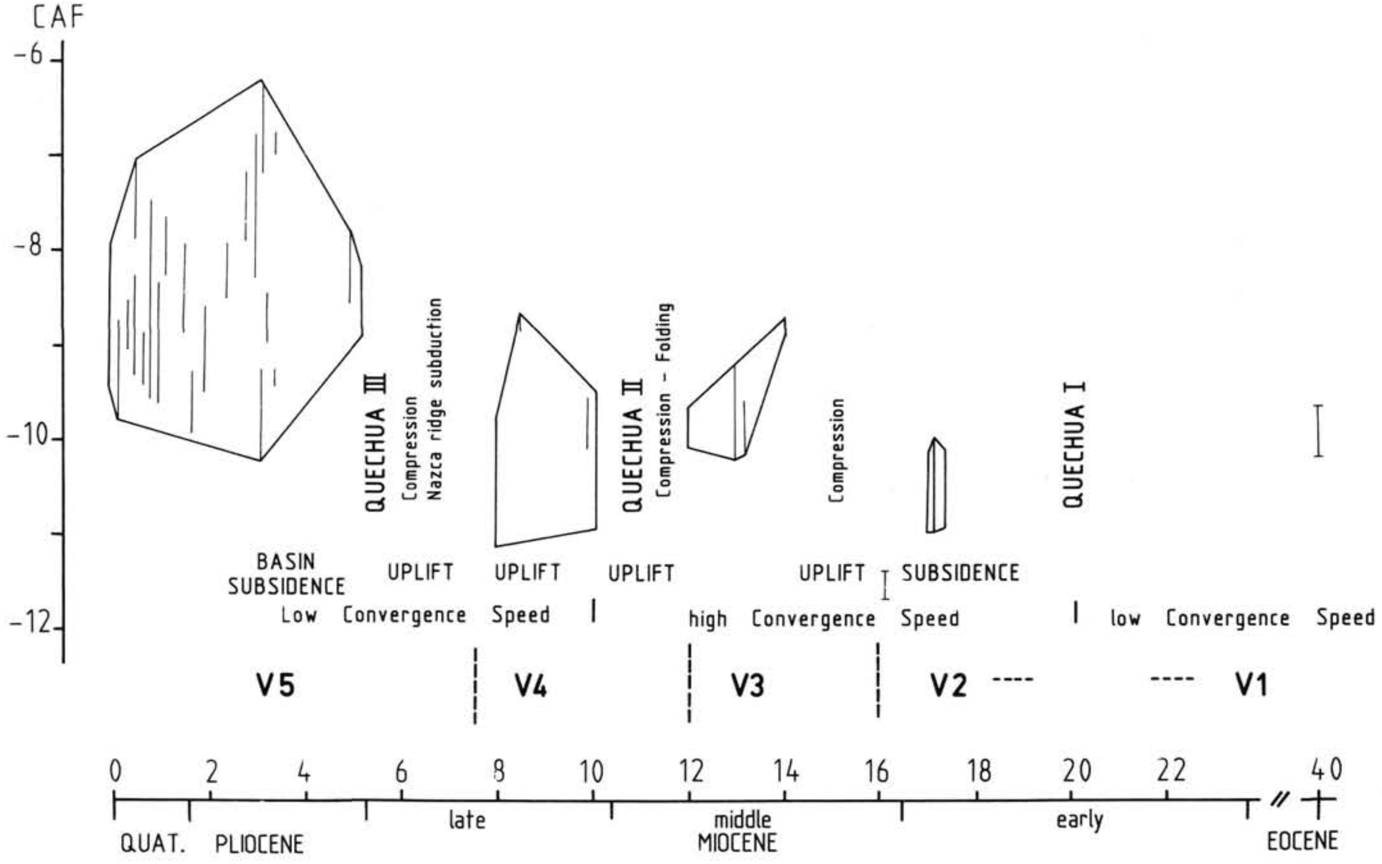

Figure 8. Volcano-tectonic events and acidic magmatic compositions (CAF) vs. time evolution.

Scarce tephra came from the northern volcanic area, by marine currents (i.e., Pleistocene L-layer); but these mainly came from southern Peru and northern Chile by aerial and marine currents.

Using volcanic pulses and variations of magmatic activity documented in Leg 112 sites, we have constructed a correlation with the volcano-tectonic history of the Andean arc, taking into account the rate and geometry of plate convergence (Engebretson et al., 1985; Pardo-Casas and Molnar, 1987). Many studies have given chronological markers (Lefèvre, 1973, 1979; Noble, 1978; Noble et al., 1974, 1979; Barazangi and Isacks, 1976; Mégard and Philip, 1976; Bourgois and Janjou, 1981; Janjou et al., 1981; McKee and Noble, 1982; von Huene, Suess, et al., 1989). The deep-sea chronological record of the explosive activity presents one a good opportunity to examine these volcano-tectonic pulses. We summarize the volcanic events (V1–V5) as follows, using Leg 112 data (Fig. 8):

V1—The oldest volcanic activity related to arc magmatism, dated Late Cretaceous to Paleocene. A mid-Eocene event was recorded in Site 683, which exhibits a moderate calc-alkaline affinity of a convergent continental margin. The late Eocene and Oligocene tectonic pulses correspond to an important sediment hiatus and to the last Incaic and first Quechua unconformity. A landward migration of the shelf has been documented (von Huene, Suess, et al, 1989). Low convergence speed and weak inclination of the subducting slab may explain the eastward migration of the Peruvian volcanic arc during early Miocene time.

V2—Early Miocene volcanic activity is contemporaneous with a new basin subsidence. Acidic ashes were recorded in Sites 683 and 688; these had a low-to-moderate calc-alkaline affinity.

V3—Mid-Miocene volcanic material occurs throughout the Leg 112 area and displays an increase of the calc-alkaline signature of a mature arc.

V4—The mid- to late Miocene tectonic pulse corresponds to the paroxysm of the Quechua event, with a change in the rate (decrease) and geometry of plate convergence. This late Miocene volcanic activity is recorded in the northern sites. Geochemical data indicate a low-to-medium calc-alkaline affinity.

V5—The late Miocene Andean orogeny (Quechua 111) is apparent throughout the Leg 112 area. In central Peru, the Nazca Ridge subduction has been proposed as responsible for the volcanic gap (Nur and Ben-Avraham, 1984). This subduction is linked to the low dipping of the slab. The underplating of material may have caused a cessation of volcanic feeding. The Andean arc experienced a general uplift of the margin and a crustal thickening. The Pliocene-Pleistocene volcanic explosive activity has been recorded mainly in the southern shelf sites. The calc-alkaline factor shows a critical change with a strong increase. This indicates a drastic modification in the conditions of magma genesis and/or magma differentiation in a thickened continental plate.

ACKNOWLEDGMENTS

We acknowledge A. Desprairies, Université de Orsay, France, for giving us samples of ash layers from the SeaPERC cruise, and the anonymous reviewers for their useful comments. This research was supported by a CNRS grant (ODP-France).

REFERENCES

Barazangi, M., and Isacks, B. L., 1976. Spacial distribution of earthquakes and subduction of the Nazca Plate beneath South America. *Geology*, 4:686–692.

Bonatti, E., and Arrhenius, G., 1970. Acidic rocks on the Pacific Ocean floor. *In* Maxwell, A. (Ed.), *The sea*, Vol. 4: New York (Wiley-Interscience), 445–464.

Bourgois, J., and Janjou, D., 1981. Subduction océanique, subduction continentale et surrection andine: l'exemple du Pérou septentrional. *C.R. Acad. Sci., Paris*, 293 sér., 11:859–864.

Bourgois, J., Pautot, G., Bandy, W., Boinet, T., Chotin, P., Huchon, P., Mercier de Lepinay, B., Monge, F., Monlau, J., Pelletier, B., Sosson, M., and von Huene, R., 1986. Régime tectonique de la marge andine convergente du Pérou (Campagne SEAPERC du *Jean Charcot*, juillet 1986). *C.R. Acad. Sci., Paris*, 303 sér., 11:1599–1604.

Bourgois, J., Pautot, G., Bandy, W., Boinet, T., Chotin, P., Huchon, P., Mercier de Lepinay, B., Monge, F., Monlau, J., Pelletier, B., Sosson, M., and von Huene, R., 1988a. Seabeam and seismic reflection imaging of the tectonic regime of the Andean continental margin off Peru (4°S to 10°S). *Earth Planet. Sci. Lett.*, 87:111–126.

Bourgois, J., von Huene, R., Pautot, G., and Huchon, P., 1988b. *Jean Charcot* Seabeam survey along ODP Leg 112 northern transect. *In* Suess, E., von Huene, R., et al., *Proc. ODP. Init. Repts.*, 112: College Station, TX (Ocean Drilling Program), 131–137.

Cadet, J.-P., and Fujioka, K., 1980. Neogene volcanic ashes and explosive volcanism: Japan trench transect, Leg 57, DSDP. *In* Scientific Party, *Init. Repts. DSDP*, 56, 57 (Pt. 2): Washington (U.S. Govt. Printing Office), 1027–1041.

Cadet, J.-P., Thisse, Y., Pouclet, A., Bardintzeff, J.-M., and Stephan, J.-F., 1981. Tephra from Deep Sea Drilling Project Leg 66: Middle America Trench transect (Southern Mexico). *In* Watkins, J. S., Moore, J. C., et al., *Init. Repts. DSDP*, 66: Washington (U.S. Govt. Printing Office), 687–698.

Cadet, J.-P., Pouclet, A., Thisse, Y., Bardintzeff, J.-M., and Azèma, J., 1982. Middle America Neogene explosive volcanism and ash layers: evidence from the Middle America Trench transect. *In* Aubouin, J., von Huene, R., et al., *Init. Repts. DSDP*, 67: Washington (U.S. Govt. Printing Office), 475–491.

Coulais, B., 1987. Les boues siliceuses à diatomées de la zone de fracture de Mendaña (fosse du Pérou), étude des carottes. Campagne SEAPERC. *Rept. DEA*: Paris (Univ. Paris XI, Orsay), 44.

Déruelle, B., 1979. Pétrologie d'un volcanisme de marge active: Atacama et Andes méridionales (Ph.D. dissert.) Université de Paris XI, Orsay.

Donnelly, T. W., 1974. Neogene explosive activity of the western Pacific: Sites 292 and 296, DSDP Leg 31. *In* Ingle, J. C., Karig, D. E., et al., *Init. Repts., DSDP*, 31: Washington (U.S. Govt. Printing Office), 577–598.

Donnelly, T. W., 1976. Tertiary explosive volcanic activity in the Eastern Equatorial Pacific Ocean: Sites 320 and 321, DSDP Leg 34. *In* Yeats, R. S., Hart, S. R., et al., *Init. Repts. DSDP*, 34: Washington (U.S. Govt. Printing Office), 605–609.

Drexler, J. W., Rose, W. I., Jr., Sparks, R.S.J., and Ledbetter, M. T., 1980. The Los Chocoyos ash, Guatemala: a major stratigraphic marker in Middle America and in three ocean basins. *Quaternary Res.*, 13:327–345.

Eberhart, J. P., and Triki, R., 1972. Description d'une technique permettant d'obtenir des coupes minces de minéraux par ultramicrotomie. Application à l'étude de minéraux argileux interstratifiés. *J. Microscopie*, 15:111–120.

Ehret, G., 1985. Une mèthode de préparation de coupes ultraminces pour l'étude en microscopie électronique des coupes d'altération formées à la surface des verres. Application a un verre bioassimilable du système SiO_2-Na_2O-CaO-P_2O_5 (DESS): Strasbourg (Université Louis Pasteur).

Engebretson, D. C., Cox, A., and Gordon, R. G., 1985. Relative motions between oceanic and continental plates in the Pacific Basin. *Geol. Soc. Am. Spec. Pap.*, 206:1–59.

Hein, J. R., and Scholl, D. W., 1978. Diagenesis and distribution of late Cenozoic volcanic sediment in the southern Bering sea. *Geol. Soc. Am. Bull.*, 89:197–210.

Hein, J. R., Scholl, D. W., and Miller, J., 1978. Episodes of Aleutian Ridge explosive volcanism. *Science*, 199:137–141.

Huang, T. C., 1980. A volcanic sedimentation model: implications of processes and responses of deep-sea ashes. *Mar. Geol.*, 38:103–122.

Hussong, D. M., Reed, T. B., and Bartlett, W. A., 1988. Seamarc II sonar imagery and bathymetry of the Nazca Plate and Peru forearc, ODP Leg 112. *In* Suess, E., von Huene, R., et al., *Proc. ODP, Init. Repts.*, 112: College Station, TX (Ocean Drilling Program), 125–130.

Imbert, T., and Desprairies, A., 1987. Neoformation of halloysite on volcanic glass in a marine environment. *Clay Minerals*, 22:179–185.

James, R. S., and Hamilton, D. L., 1969. Phase relations in the system $NaAlSi_3O_8$-$KAlSi_3O_8$-$CaAl_2Si_2O_8$-SiO_2 at 1 kb water vapor pressure. *Contr. Mineral. Petrol.*, 21:111–141.

Janjou, D., Bourgois, J., Mégard, F., and Sornay, J., 1981. Rapports paléogéographiques et structuraux entre Cordillères occidentale et orientale des Andes nord péruviennes: les écailles du Maranon (7°S, Département de Cajamarca et de Amazonas, Pérou). *Bull. Soc. Geol. France*, (7), XXIII, 6:697–705.

Kennett, J. P., and Thunell, R. C., 1975. Global increase in Quaternary explosive volcanism. *Science*, 187:497–503.

Kudo, A. M., and Weill, D. F., 1970. An igneous plagioclase thermometer. *Contr. Mineral. Petrol.*, 25:52–65.

Lebart, L., Morsineau, A., and Fénélon, J. P., 1979. *Traitement des données statistiques*: Paris (Dunod Ed.).

Lefèvre, C., 1973. Les caractères magmatiques du volcanisme plioquaternaire des Andes dans le sud du Pérou. *Contr. Mineral. Petrol.*, 41:259–272.

_______, 1979. Un exemple de volcanisme de marge active dans les Andes du Pérou (sud) du Miocène a l'actuel (Ph.D. dissert.). Université de Montpellier.

Mathez, E. A., 1973. Refinment of the Kudo-Weill plagioclase thermometer and its applications to basaltic rocks. *Contr. Mineral. Petrol.*, 41:61–72.

McKee, E. H., and Noble, D. C., 1982. Miocene volcanism and deformation in the western cordillera and high plateaus of south-central Peru. *Geol. Soc. Am. Bull.*, 93:657–662.

Mégard, F., and Philip, H., 1976. Plio-Quaternary tectono-magmatic zonation and plate tectonics in the central Andes. *Earth Planet. Sci. Lett.*, 33:231–238.

Ninkovich, D., 1979. Distribution and chemical composition of tephra layers in deep sea sediments off western Indonesia. *J. Volcanol. Geotherm. Res.*, 5:67–86.

Ninkovich, D., and Donn, W. L., 1976. Explosive Cenozoic volcanism and climatic implications. *Science*, 194:899–906.

Ninkovich, D., and Schackleton, N. S., 1975. Distribution, stratigraphy and age of ash layer "L," in the Panama Basin region. *Earth Planet. Sci. Lett.*, 27:20–34.

Noble, D. C., 1978. Cenozoic volcanism and tectonic evolution of the Andes of Peru. Summary of on-land geologic data. *EOS, Trans. Am. Geophys. Un.*, 59 (4):383.

Noble, D. C., McKee, E. H., Farrar, E., and Petersen, U., 1974. Episodic Cenozoic volcanism and tectonism in the Andes of Peru. *Earth Planet. Sci. Lett.*, 21:213–220.

Noble, D. C., McKee, E. H., and Mégard, F., 1979. Early Tertiary "Incaic" tectonism, uplift and volcanic activity, Andes of Central Peru. *Geol. Soc. Am. Bull.*, 90:903–907.

Nur, A., and Ben-Avraham, Z., 1984. Volcanic gaps and the consumption of aseismic ridges in South America. *Geol. Soc. Am. Mem.*, 154:729–740.

Pardo-Casas, F., and Molnar, P., 1987. Relative motion of the Nazca (Farallon) and South American plates since Late Cretaceous time. *Tectonics*. 6(3):233–248.

Pautot, G., Bourgois, J., Bandy, W., Boinet, T., Chotin, P., Huchon, P., Mercier de Lepinay, B., Monge, F., and Monlau, J., Pelletier, B., Sosson, M., and von Huene, R., 1986. Fragmentation de la plaque Nazca a l'Ouest de la fosse du Pérou: résultats de la campagne SEAPERC du N.0. *Jean-Charcot*, juillet 1986. *C.R. Acad. Sci., Paris*, 303 sér. II, 18:1651–1656.

Pouclet, A., Cadet, J.-P., Fujioka, K., and Bourgois, J., 1985a. Ash layers from Deep Sea Drilling Project Leg 84: Middle America Trench transect. *In* von Huene, R., Aubouin, J., et al., *Init. Repts. DSDP*, 84: Washington (U.S. Govt. Printing Office), 609–618.

Pouclet, A., Fujioka, K., Charvet, J., and Cadet, J.-P., 1986b. Petrography and geochemistry of volcanic ash layers from Leg 87A, Nankai Trough (South Japan). *In* Kagami, H., Karig, D. E., Coulbourn, W. T., et al., *Init. Repts. DSDP*, 87: Washington Govt. Printing Office), 695–701.

Scheidegger, K. F., Jezek, P. A., and Ninkovich, D., 1978. Chemical and optical studies of glass shards in Pleistocene and Pliocene ash layers from DSDP Site 192, northern Pacific Ocean. *J. Volcanol. Geotherm. Res.*, 4:99–116.

Suess, E., von Huene, R., and the Leg 112 Shipboard Scientific Party, 1989. ODP Leg 112: the Peru continental margin—II History and geochemistry of depositional environment. *In* Suess, E., von Huene, R., et al., *Proc. ODP, Init. Repts.*, 112: College Station, TX (Ocean Drilling Program).

Thomassin, J.-H., 1984. Etude expérimentale de l'altération des verres silicatés dans l'eau douce et en milieu océanique. Apport des méthodes d'analyse de surface des solides (Ph.D. dissert.) Université d'Orléans.

von Huene, R., Suess, E., and the Leg 112 Shipboard Scientific Party, 1989. Results of Leg 112 drilling, Peru continental margin: part 1, tectonic history. *In* Suess, E., von Huene, R., et al., *Proc. ODP, Init. Repts.*, 112: College Station, TX (Ocean Drilling Program).

Wones, D. R., and Eugster, H. P., 1965. Stability of biotite: experiment, theory and application. *Am. Mineral.,* 50:1228–1272.

Woodruff, L. E., Rose, W. I., Jr., and Rigot, W., 1979. Contrasting fractionation patterns for sequential magmas from two calc-alkaline volcanoes in Central America. *J. Volcanol. Geotherm. Res.*, 6:217–240.

Yeats, R. S., Hart, S. R., et al., 1976. *Init. Repts. DSDP*, 34: Washington (U S. Govt. Printing Office).

Date of initial receipt: 12 December 1988
Date of acceptance: 5 July 1989
Ms 112B-167